PHYSICAL REVIEW B **88**, 161406(R) (2013)

Topological Kirchhoff law and bulk-edge correspondence for valley Chern and spin-valley Chern numbers

Motohiko Ezawa
Department of Applied Physics, University of Tokyo, Hongo 7-3-1, 113-8656 Tokyo, Japan
(Received 19 August 2013; published 22 October 2013)

The valley Chern and spin-valley Chern numbers are the key concepts in valleytronics. They are topological numbers in the Dirac theory but not in the tight-binding model. We analyze the bulk-edge correspondence between the two phases which have the same Chern and spin-Chern numbers but different valley Chern and spin-valley Chern numbers. Though the edge state between them is topologically trivial in the tight-binding model, it is shown to be as robust as the topological one both for zigzag and armchair edges. We construct Y-junctions made of topological edges. They satisfy the topological Kirchhoff law, where the topological charges are conserved at the junction. We may interpret a Y-junction as a scattering process of particles which have four topological numbers. It would be a milestone of future topological electronics.

DOI: 10.1103/PhysRevB.88.161406 PACS number(s): 03.65.Vf, 73.22.Pr, 02.40.Pc, 71.70.Ej

I. INTRODUCTION

Topological insulators are one of the most fascinating concepts discovered in this decade.[1,2] A topological insulator is characterized by topological indices such as the Chern number $\mathcal{C}$ and the $\mathbb{Z}_2$ index. When the spin s_z is a good quantum number, the spin-Chern number $\mathcal{C}_s$ replaces the role of the $\mathbb{Z}_2$ index.[3–5] We consider honeycomb lattice systems. Electrons reside either in the K or K' valley in the low-energy physics subject to the Dirac theory. Accordingly, we can define the valley Chern number[6–8] $\mathcal{C}_v$ and the spin-valley Chern number[6] $\mathcal{C}_{sv}$ in the Dirac theory. This valley degree of freedom leads to valleytronics.[9–20] On the other hand, $\mathcal{C}$ and $\mathcal{C}_s$ are independent of the valley degree of freedom since they are defined by the summation of Berry curvatures over the entire Brillouin zone. Namely, a state is indexed by the two topological numbers in the tight-binding model, while it is indexed by the four topological numbers in the Dirac theory.

There are four independent spin-valley-dependent Chern numbers in the Dirac theory of honeycomb systems. Each Chern number can be controlled independently by changing the sign of spin-valley-dependent Dirac masses. There are 16 types of topological insulators, as shown in Table I. They are the quantum anomalous Hall (QAH) insulator, four types of spin-polarized QAH (SQAH) insulators, the quantum spin Hall (QSH) insulator, and the band insulator with charge-density-wave (CDW) or antiferromagnetic (AF) order. The CDW and AF insulators are regarded as trivial in the tight-binding model.

In this paper, we study the bulk-edge correspondence with respect to $\mathcal{C}_v$ and $\mathcal{C}_{sv}$ by examining the boundary of two insulators which have the same $\mathcal{C}$ and $\mathcal{C}_s$ but different $\mathcal{C}_v$ and $\mathcal{C}_{sv}$. We show that gapless edge states appear along the boundary, although they are trivial in the tight-binding model. Furthermore, we show that they are as robust as the topologically protected edges both for zigzag and armchair edges.

We propose a topological electronics based on the edge states in the Dirac theory. We are able to assign four topological numbers $\mathcal{C}$, $\mathcal{C}_s$, $\mathcal{C}_v$, and $\mathcal{C}_{sv}$ to each edge state. By joining three different topological insulators at one point, we can construct a Y-junction made of topological edge states. The edge states at the junction satisfy the conservation of four topological numbers, which we call the topological Kirchhoff law. We can change the connectivity of edge states by changing the topological property of bulk insulators, for instance by applying an electric field. The process may be interpreted as a pair annihilation of two Y-junctions.

II. HAMILTONIAN

The honeycomb lattice consists of two sublattices made of A and B sites. We consider a buckled system with the layer separation 2ℓ between these two sublattices. The states near the Fermi energy are π orbitals residing near the K and K' points at opposite corners of the hexagonal Brillouin zone. The low-energy dynamics in the K and K' valleys is described by the Dirac theory. In what follows, we use notations $s_z = \uparrow, \downarrow$, $t_z = A, B$, $\eta = K, K'$ in indices while $s_z^\alpha = \pm 1$ for $\alpha = \uparrow, \downarrow$, $t_z^i = \pm 1$ for $i = A, B$, and $\eta_i = \pm 1$ for $i = K, K'$ in equations. We also use the Pauli matrices σ_a and τ_a for the spin and the sublattice pseudospin, respectively.

We have previously proposed a generic Hamiltonian for honeycomb systems,[21] which contains eight interaction terms mutually commutative in the Dirac limit. Among them, four contribute to the Dirac mass. The other four contribute to the shift of the energy spectrum. We are able to fully control the Dirac mass and the energy shift independently at each spin and valley by varying these parameters, and materialize various topological phases.[22,23]

By taking those affecting the Dirac mass, the tight-binding model is given by[21,24,25]

$$\begin{aligned} H = & -t \sum_{\langle i,j\rangle\alpha} c_{i\alpha}^\dagger c_{j\alpha} + i\frac{\lambda_{\rm SO}}{3\sqrt{3}} \sum_{\langle\langle i,j\rangle\rangle\alpha\beta} \nu_{ij} c_{i\alpha}^\dagger \sigma_{\alpha\beta}^z c_{j\beta} \\ & - \lambda_V \sum_{i\alpha} \mu_i c_{i\alpha}^\dagger c_{i\alpha} + i\frac{\lambda_\Omega}{3\sqrt{3}} \sum_{\langle\langle i,j\rangle\rangle\alpha\beta} \nu_{ij} c_{i\alpha}^\dagger c_{j\beta} \\ & + \lambda_{\rm SX} \sum_{i\alpha} \mu_i c_{i\alpha}^\dagger \sigma_{\alpha\alpha}^z c_{i\alpha}, \end{aligned} \tag{1}$$

where $c_{i\alpha}^\dagger$ creates an electron with spin polarization α at site i, and $\langle i,j\rangle/\langle\langle i,j\rangle\rangle$ run over all the nearest/next-nearest-neighbor hopping sites. We explain each term. The first term represents the nearest-neighbor hopping with the transfer energy t. The

TABLE I. Corresponding to the spin and valley degrees of freedom, there are four Chern numbers $\mathcal{C}^{\eta}_{s_z}$, each of which takes $\pm\frac{1}{2}$. Equivalently they are given by the Chern ($\mathcal{C}$), spin Chern ($\mathcal{C}_s$), valley Chern ($\mathcal{C}_v$), and spin-valley Chern ($\mathcal{C}_{sv}$) numbers. Hence there are 16 states indexed by them, among which eight states are explicitly displayed. The other eight states are the conjugate states such as QAH* with $-\mathcal{C}^{\eta}_{s_z}$ for QAH with $\mathcal{C}^{\eta}_{s_z}$.

	$C^K_\uparrow$	$C^{K'}_\uparrow$	$C^K_\downarrow$	$C^{K'}_\downarrow$	C	$2C_s$	C_v	$2C_{sv}$
QAH	1/2	1/2	1/2	1/2	2	0	0	0
SQAH_1	1/2	1/2	1/2	−1/2	1	1	1	−1
SQAH_2	1/2	−1/2	1/2	1/2	1	1	−1	1
SQAH_3	1/2	1/2	−1/2	1/2	1	−1	1	1
SQAH_4	−1/2	1/2	1/2	1/2	1	−1	−1	−1
QSH	1/2	−1/2	1/2	−1/2	0	2	0	0
CDW	1/2	1/2	−1/2	−1/2	0	0	2	0
AF	1/2	−1/2	−1/2	1/2	0	0	0	2

second term represents the SO coupling[24] with λ_{SO}. The third term is the staggered sublattice potential term[26] with $\lambda_V = \ell E_z$ in electric field E_z. The fourth term is the Haldane term[27] with λ_Ω. The fifth term represents the antiferromagnetic exchange magnetization[21,28] with λ_{SX}.

We give typical sample parameters, although we treat them as free parameters. Silicene is a good candidate, where $t = 1.6$ eV, $\lambda_{\text{SO}} = 3.9$ meV, and $\ell = 0.23$ Å. The Haldane term might be induced by the photoirradiation, where $\lambda_\Omega = \hbar v_{\text{F}}^2 \mathcal{A}^2 \Omega^{-1}$, with Ω the frequency and $\mathcal{A}$ the dimensionless intensity.[23,29,30] The antiferromagnetic exchange magnetization might be induced by certain proximity effects. The second candidate is perovskite transition-metal oxide grown in the [111] direction, which has antiferromagnetic order intrinsically.[31] This material also has a buckled structure, as in the case of silicene. Parameters are $t \approx 0.2$ eV, $\lambda_{\text{SO}} = 7.3$ meV, $\lambda_V = \ell E_z$, and $\lambda_{\text{SX}} = 141$ meV for LaCrAgO.

The low-energy Hamiltonian is described by[21]

$$H_\eta = \hbar v_{\text{F}}(\eta k_x \tau_x + k_y \tau_y) + \lambda_{\text{SO}} \sigma_z \eta \tau_z - \lambda_V \tau_z + \lambda_\Omega \eta \tau_z + \lambda_{\text{SX}} \sigma_z \tau_z, \tag{2}$$

where $v_{\text{F}} = \frac{\sqrt{3}}{2\hbar} at$ is the Fermi velocity. The coefficient of τ_z is the mass of Dirac fermions in the Hamiltonian,

$$\Delta^{\eta}_{s_z} = \eta s_z \lambda_{\text{SO}} - \lambda_V + \eta \lambda_\Omega + s_z \lambda_{\text{SX}}. \tag{3}$$

The band gap is given by $2|\Delta^{\eta}_{s_z}|$.

III. TOPOLOGICAL NUMBERS

We consider the systems in which the spin s_z is a good quantum number. The summation of the Berry curvature over all occupied states of electrons with spin s_z in the Dirac valley K_η yields[1,2,32]

$$\mathcal{C}^{\eta}_{s_z} = \frac{\eta}{2} \text{sgn}\left(\Delta^{\eta}_{s_z}\right). \tag{4}$$

There are four independent spin-valley-dependent Dirac masses determined by the four parameters λ_{SO}, λ_V, λ_Ω, and λ_{SX}. Accordingly, we can define

$$\mathcal{C} = \mathcal{C}^K_\uparrow + \mathcal{C}^{K'}_\uparrow + \mathcal{C}^K_\downarrow + \mathcal{C}^{K'}_\downarrow, \tag{5}$$

$$\mathcal{C}_s = \tfrac{1}{2}(\mathcal{C}^K_\uparrow + \mathcal{C}^{K'}_\uparrow - \mathcal{C}^K_\downarrow - \mathcal{C}^{K'}_\downarrow), \tag{6}$$

and

$$\mathcal{C}_v = \mathcal{C}^K_\uparrow - \mathcal{C}^{K'}_\uparrow + \mathcal{C}^K_\downarrow - \mathcal{C}^{K'}_\downarrow, \tag{7}$$

$$\mathcal{C}_{sv} = \tfrac{1}{2}(\mathcal{C}^K_\uparrow - \mathcal{C}^{K'}_\uparrow - \mathcal{C}^K_\downarrow + \mathcal{C}^{K'}_\downarrow). \tag{8}$$

It should be emphasized that $\mathcal{C}_v$ and $\mathcal{C}_{sv}$ are not defined in the tight-binding model.

The possible sets of topological numbers are $(\mathcal{C},\mathcal{C}_s) = (0,0)$, $(2,0)$, $(0,1)$, $(1,\frac{1}{2})$, $(1,-\frac{1}{2})$ up to the overall sign $\pm$ in the tight-binding model. They are the trivial, QAH, QSH, and two types of SQAH insulators, respectively. They are further classified into subsets according to the valley degree of freedom in the Dirac theory. Trivial insulators are divided into two: one with CDW order and the other with AF orders.[21] Each type of SQAH insulator is divided into two: There are four types in all, which we denote by SQAH_i, with $i = 1,2,3,4$. All of them are summarized in Table I.

IV. BULK-EDGE CORRESPONDENCE

The most convenient way to determine the topological charges is to employ the bulk-edge correspondence. When there are two topologically distinct phases, a topological phase transition may occur between them. The band gap must close at the topological phase-transition point since the topological number cannot change its quantized value without closing the gap. Note that the topological number is only defined in the gapped system and remains unchanged for any adiabatic process. Alternatively, we may consider a boundary separating two different topological phases in a single honeycomb system.[26] Gapless edge modes must appear along the phase boundary. Let us investigate typical examples. Similar results are obtained from all other cases.

V. CDW-CDW* JUNCTION

We first investigate a trivial insulator in the tight-binding model. We take an example of a CDW with $(0,0,2,0)$ or a CDW* with $(0,0,-2,0)$. A nanoribbon made of either the CDW insulator or the CDW* insulator has no gapless edge modes, which is regarded as being a demonstration of their triviality: See Fig. 1(b) for a zigzag nanoribbon and Fig. 1(c) for an armchair nanoribbon. One may wonder how they can be topological in the Dirac theory without gapless edge modes in view of the bulk-edge correspondence. The answer to this problem is that $\mathcal{C}_v$ and $\mathcal{C}_{sv}$ are not defined in the vacuum. The gap need not close at such a boundary because $\mathcal{C}_v$ and $\mathcal{C}_{sv}$ are defined only inside of the nanoribbon. This explains the absence of gapless edge modes.

We next investigate a boundary made of a CDW with $(0,0,2,0)$ and a CDW* with $(0,0,-2,0)$ in a single honeycomb system.[26] We refer to edge modes along the boundary as inner-edge modes in order to distinguish them from the ordinary edge modes along a boundary separating the material and the vacuum. We have calculated the band structure of a hybrid nanoribbon by separating a nanoribbon into two parts, one in the CDW phase and the other in the CDW* phase: See Fig. 1(d). Only $\mathcal{C}_v$ changes across the boundary separating these two phases. The phase boundary is a CDW domain wall with the CDW order reversed at a line defect. Let us take the line along the x axis. The domain wall is well described by $\lambda_V(y) = \lambda_V \tanh(y/\xi)$ with the domain-wall width ξ. The

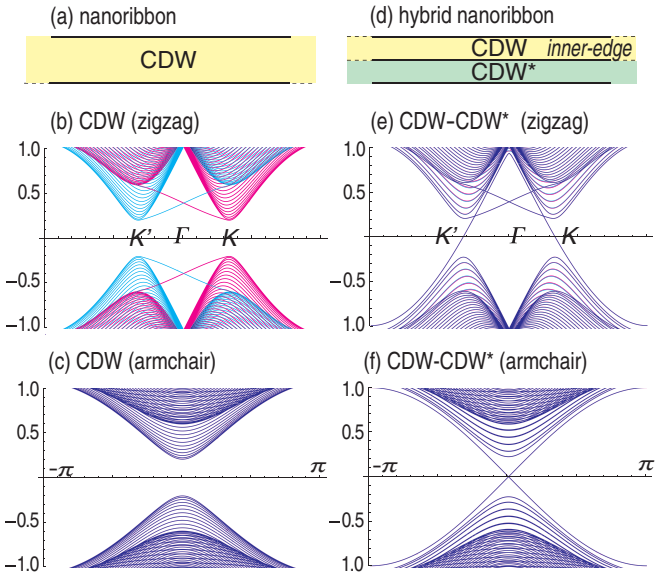

FIG. 1. (Color online) Illustration of (a) a nanoribbon and (d) a hybrid nanoribbon. Band structures of a nanoribbon made of a CDW insulator for (b) zigzag and (c) armchair edges. Band structures of a hybrid nanoribbon made of CDW-CDW* insulators for (e) zigzag and (f) armchair inner edges. Up, down, and degenerate spin bands are shown in magenta, cyan, and violet, respectively. For illustration, we have taken $\lambda_{SO} = 0.2t$ and $|\lambda_V| = 0.4t$; the domain-wall width $\xi = a$ and the nanoribbon width $w = 28a$ for the zigzag edge; and $w = 50.5a$ for the armchair edge. Typical structures remain as they are for realistic values.

band structure of a hybrid nanoribbon is given for a zigzag nanoribbon in Fig. 1(e) and for an armchair nanoribbon in Fig. 1(f). It is insensitive to the domain-wall width ξ provided it is much smaller than the width w of a nanoribbon.

We find one inner-edge state crossing the Fermi energy twice in the band structure of the zigzag boundary in Fig. 1(e), where up-spin and down-spin states are degenerate. It is highly enhanced at the Γ point, where it almost touches the bulk band. This implies that the inner-edge state is almost as robust as a topologically protected state. Note that the topologically protected phase is stable against perturbation whose energy scale is less than the SO interaction energy λ_{SO}. We have checked that the band structure is insensitive to the width of a nanoribbon. This is in agreement with the analysis[33] of a helical zigzag edge channel, where the penetration depth of the channel is as short as the lattice constant.

We also examine inner-edge states in the band structure of the armchair boundary [Fig. 1(f)]. The inner-edge state is almost as robust as a topologically protected one also for the armchair boundary. We have checked that the band structure is insensitive to the width of a nanoribbon provided it is reasonably wide. This is in agreement with the analysis[33] of a helical armchair edge channel, where the interference occurs between two edge states when the width is too narrow due to a relatively large penetration depth of the channel.

VI. SQAH-SQAH JUNCTION

We next investigate the junction made of two different SQAHs. As an example, we take $SQAH_3$ with $(\mathcal{C},\mathcal{C}_s,\mathcal{C}_v,\mathcal{C}_{sv}) = (1,-1,1,1)$ and $SQAH_4$ with $(1,-1,-1,-1)$. It is not appropriate to use a hybrid nanoribbon in the present case since gapless edge modes appear even for a simple nanoribbon in the SQAH phase. We calculate the band structure of a nanotube geometry since no gapless edge modes appear even for a simple nanotube in the SQAH phase due to the lack of the edge itself: See Fig. 2(b) for a zigzag nanotube and Fig. 2(c) for an armchair nanotube. We calculate the band structure of a hybrid nanotube where one-half of the nanotube is $SQAH_3$ and the other half is $SQAH_4$, as illustrated in Fig. 2(d). We see clearly a gapless inner-edge mode highly enhanced at the Γ point for the zigzag boundary in Fig. 2(e) and at $k = \pm\pi$ for the armchair boundary in Fig. 2(f). The inner-edge state is almost as robust as a topologically protected one also in this case.

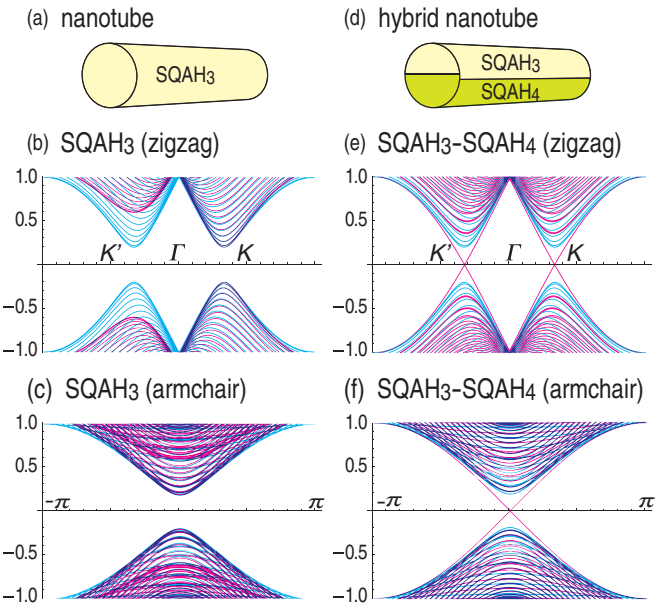

FIG. 2. (Color online) Illustration of (a) a nanotube and (d) a hybrid nanotube. Band structures of a nanotube made of a $SQAH_3$ insulator for (b) zigzag and (c) armchair edges. Band structures of a hybrid nanotube made of $SQAH_3$ and $SQAH_4$ for (e) zigzag and (f) armchair inner edges. We have taken $\lambda_{SO} = |\lambda_V| = |\lambda_{SX}| = 0.2t$ for illustration. See also the caption of Fig. 1.

VII. GAPLESS EDGE MODE IN DIRAC THEORY

We proceed to construct the Dirac theory of gapless inner-edge states.[26] They emerge along a curve where the Dirac mass vanishes, $\Delta^{\eta}_{s_z}(x,y) = 0$. Let us take the edge along the x axis. The zero modes emerge along the line determined by $\Delta^{\eta}_{s_z}(y) = 0$, when $\Delta^{\eta}_{s_z}(y)$ changes sign. We may set $k_x = \text{const}$ due to the translational invariance along the x axis. We seek the zero-energy solution by setting $\psi_B = i\zeta\psi_A$ with $\zeta = \pm 1$. Here, ψ_A is a two-component amplitude with the up spin and down spin, $\psi_A = (\psi^{\uparrow}_A, \psi^{\downarrow}_A)$. Setting $\psi_A(x,y) = e^{ik_x x}\phi_A(y)$, we obtain $H_\eta\psi_A(x,y) = E_{\eta\zeta}\psi_A(x,y)$, together with a linear dispersion relation $E_{\eta\zeta} = \eta\zeta\hbar v_F k_x$. We can explicitly solve this as

$$\phi_A(y) = C\exp\left[\frac{\zeta}{\hbar v_F}\int^{y}\Delta^{\eta}_{s_z}(y')\,dy'\right], \qquad (9)$$

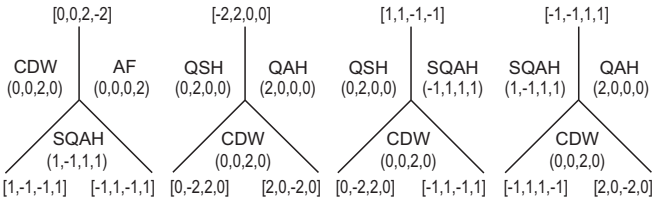

FIG. 3. Illustrations of typical Y-junctions. The edge between two different topological insulators carries a set of four topological charges. Three edges can make a Y-junction provided that the sum of their topological charges is zero.

where C is the normalization constant. The sign ζ is determined so as to make the wave function finite in the limit $|y| \to \infty$. This is reminiscent of the Jackiw-Rebbi mode[34] presented for the chiral mode. The difference is the presence of the spin and valley indices in the wave function.

VIII. TOPOLOGICAL KIRCHHOFF LAW

We consider a configuration where three different topological insulators meet at one point: see Fig. 3. In this configuration, there are three edges forming a Y-junction. It is convenient to assign the topological numbers to each edge, which are the difference between those of the two adjacent topological insulators. Namely, when the topological insulator with $(\mathcal{C}^L,\mathcal{C}_s^L,\mathcal{C}_v^L,\mathcal{C}_{sv}^L)$ is on the left-hand side of the one with $(\mathcal{C}^R,\mathcal{C}_s^R,\mathcal{C}_v^R,\mathcal{C}_{sv}^R)$, we assign the numbers $[\mathcal{C}^L-\mathcal{C}^R,\mathcal{C}_s^L-\mathcal{C}_s^R,\mathcal{C}_v^L-\mathcal{C}_v^R,\mathcal{C}_{sv}^L-\mathcal{C}_{sv}^R]$ to the boundary, as illustrated in Fig. 3. The condition under which edges can make a Y-junction is the conservation of these topological numbers at the junction. This law is reminiscent of the Kirchhoff law, which dictates the conservation of currents at the junction of electronic circuits. We call it the topological Kirchhoff law.

The number of Y-junctions is given by the combination of selecting 3 from 16 topological insulators, i.e., ${}_{16}C_3 = 560$. The number of topological edge states is determined by the combination of selecting 2 from 16 topological insulators. We have ${}_{16}C_2 = 120$ types of topological edge states. We show typical examples of Y-junctions in Fig. 3.

We present an interesting interpretation of the topological Kirchhoff law. We may regard each topological edge state as a world line of a particle carrying the four topological charges. The Y-junction may be interpreted as a scattering process of these particles. In this scattering process, the topological charges conserve.

IX. TOPOLOGICAL ELECTRONIC CIRCUITS

We can construct electronic circuits made of edge states by joining Y-junctions. Each topological edge state carries conductance,[35] whose magnitude is given by the Chern number $\mathcal{C}$ in units of e^2/h. The present-day electronic circuits only use this charge degree of freedom. In our circuits of topological edges, we can make full use of four types of charges: $\mathcal{C}, \mathcal{C}_s, \mathcal{C}_v$, and $\mathcal{C}_{sv}$. This would greatly enhance the ability of information processing.

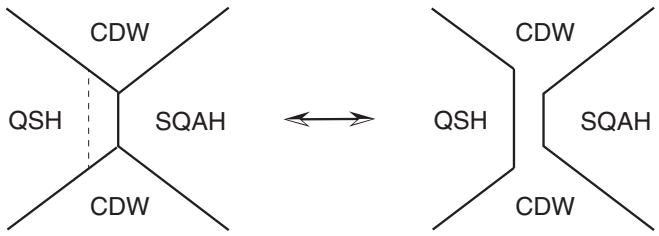

FIG. 4. Schematic illustration of a topological electronic circuit. The CDW phase is created by applying electric field E_z to the QSH phase beyond the critical value $E_{\rm cr}$. Tuning it locally, we can change the form of the circuit by a pair annihilation of two Y-junctions.

We can control the position of the edge state by controlling the parameters of the bulk states. The easiest way is to apply electric field E_z locally. Let us review the topological phase transition taking place as E_z changes[26] by taking $\lambda_\Omega = \lambda_{\rm SX} = 0$, where the Dirac mass is given by $\Delta_{s_z}^\eta = \eta s_z \lambda_{\rm SO} - \ell E_z$. The condition $\Delta_{s_z}^\eta = 0$ implies $E_z = \pm E_{\rm cr}$ with $E_{\rm cr} = \lambda_{\rm SO}/\ell$. It follows that $(\mathcal{C},\mathcal{C}_s) = (0,0)$ for $|E_z| < E_{\rm cr}$ and $(0,\frac{1}{2})$ for $|E_z| > E_{\rm cr}$. For instance, the two CDW domains are made in this way in Fig. 4(a). Applying E_z only to a part in the QSH domain near the SQAH domain, we can turn this part into the CDW domain as in Fig. 4(b). We have thus changed the form of the circuit by a pair annihilation of two Y-junction by applying E_z. This will pave the way for topological electronics.

X. DISCUSSION

We have proposed a network of inner-edge states appearing along boundaries separating different topological phases in a single honeycomb system. They carry charges $\mathcal{C}$, $\mathcal{C}_s$, $\mathcal{C}_v$, and $\mathcal{C}_{sv}$. They are topological charges in the low-energy Dirac theory. The phase boundaries as well as these topological phases are as robust as the genuine topological ones in the tight-binding model. When there are impurities or edge disorder on a boundary, the current detours around them by penetrating into the bulk, and the topological conservation law is maintained. We have already found such a detour along a rough edge by numerical computations for the helical edge current.[36]

ACKNOWLEDGMENTS

I am very grateful to N. Nagaosa for many fruitful discussions on the subject. This work was supported in part by Grants-in-Aid for Scientific Research from the Ministry of Education, Science, Sports and Culture No. 25400317.

[1] M. Z. Hasan and C. Kane, Rev. Mod. Phys. **82**, 3045 (2010).
[2] X.-L. Qi and S.-C. Zhang, Rev. Mod. Phys. **83**, 1057 (2011).
[3] E. Prodan, Phys. Rev. B **80**, 125327 (2009).
[4] D. N. Sheng, Z. Y. Weng, L. Sheng, and F. D. M. Haldane, Phys. Rev. Lett. **97**, 036808 (2006).
[5] Y. Yang, Z. Xu, L. Sheng, B. Wang, D. Y. Xing, and D. N. Sheng, Phys. Rev. Lett. **107**, 066602 (2011).

[6]F. Zhang, J. Jung, G. A. Fiete, Q. Niu, and A. H. MacDonald, Phys. Rev. Lett. **106**, 156801 (2011).
[7]F. Zhang, A. H. MacDonald, and E. J. Mele, Proc. Natl. Acad. Sci. (USA) **110**, 10546 (2013).
[8]J. Li, A. F. Morpurgo, M. Büttiker, and I. Martin, Phys. Rev. B **82**, 245404 (2010).
[9]A. Rycerz, J. Tworzydo, and C. W. J. Beenakker, Nat. Phys. **3**, 172 (2007).
[10]Z. Qiao, S. A. Yang, W. Feng, W.-K. Tse, J. Ding, Y. Yao, J. Wang, and Q. Niu, Phys. Rev. B **82**, 161414(R) (2010).
[11]Z. Qiao, S. A. Yang, B. Wang, Y. Yao, and Q. Niu, Phys. Rev. B **84**, 035431 (2011).
[12]Z. Qiao, H. Jiang, X. Li, Y. Yao, and Q. Niu, Phys. Rev. B **85**, 115439 (2012).
[13]Z. Qiao, X. Li, W.-K. Tse, H. Jiang, Y. Yao, and Q. Niu, Phys. Rev. B **87**, 125405 (2013).
[14]D. Xiao, W. Yao, and Q. Niu, Phys. Rev. Lett. **99**, 236809 (2007).
[15]D. Xiao, G.-B. Liu, W. Feng, X. Xu, and W. Yao, Phys. Rev. Lett. **108**, 196802 (2012).
[16]T. Cao, J. Feng, J. Shi, Q. Niu, and E. Wang, Nat. Commun. **3**, 887 (2012).
[17]J. Jung, F. Zhang, Z. Qiao, and A. H. MacDonald, Phys. Rev. B **84**, 075418 (2011).
[18]W. Yao, D. Xiao, and Q. Niu, Phys. Rev. B **77**, 235406 (2008).
[19]W.-K. Tse, Z. Qiao, Y. Yao, A. H. MacDonald, and Q. Niu, Phys. Rev. B **83**, 155447 (2011).
[20]J. Ding, Z. Qiao, W. Feng, Y. Yao, and Q. Niu, Phys. Rev. B **84**, 195444 (2011).
[21]M. Ezawa, Phys. Rev. B **87**, 155415 (2013).
[22]M. Ezawa, Phys. Rev. Lett. **109**, 055502 (2012).
[23]M. Ezawa, Phys. Rev. Lett. **110**, 026603 (2013).
[24]C. L. Kane and E. J. Mele, Phys. Rev. Lett. **95**, 226801 (2005).
[25]C.-C. Liu, H. Jiang, and Y. Yao, Phys. Rev. B **84**, 195430 (2011).
[26]M. Ezawa, New J. Phys. **14**, 033003 (2012).
[27]F. D. M. Haldane, Phys. Rev. Lett. **61**, 2015 (1988).
[28]X. Li, T. Cao, Q. Niu, J. Shi, and J. Feng, Proc. Natl. Acad. Sci. (USA) **110**, 3738 (2013).
[29]T. Kitagawa, T. Oka, A. Brataas, L. Fu, and E. Demler, Phys. Rev. B **84**, 235108 (2011).
[30]T. Oka and H. Aoki, Phys. Rev. B **79**, 081406(R) (2009).
[31]Q.-F. Liang, L.-H. Wu, and X. Hu, New J. Phys. **15**, 063031 (2013).
[32]M. Ezawa, Europhys. J. B **85**, 363 (2012).
[33]M. Ezawa and N. Nagaosa, Phys. Rev. B **88**, 121401(R) (2013).
[34]R. Jackiw and C. Rebbi, Phys. Rev. D **13**, 3398 (1976).
[35]M. Ezawa, Appl. Phys. Lett. **102**, 172103 (2013).
[36]K. Kikutake, M. Ezawa, and N. Nagaosa, Phys. Rev. B **88**, 115432 (2013).